ACS OMEGA

Article

http://pubs.acs.org/journal/acsodf

Silver Nanowire/Carbon Sheet Composites for Electrochemical Syngas Generation with Tunable H_2/CO Ratios

Minhyung Cho,[†] Ji-Won Seo,[†,‡] Jun Tae Song,[†,§] Jung-Yong Lee,*[,†,§] and Jihun Oh*[,†,§]

[†]Graduate School of Energy, Environment, Water, and Sustainability (EEWS), [‡]Information & Electronics Research Institute, and [§]KAIST Institute for NanoCentury, Korea Advanced Institute of Science and Technology (KAIST), Daejeon 34141, Republic of Korea

Supporting Information

ABSTRACT: Generating syngas (H_2 and CO mixture) from electrochemically reduced CO_2 in an aqueous solution is one of the sustainable strategies utilizing atmospheric CO_2 in value-added products. However, a conventional single-component metal catalyst, such as Ag, Au, or Zn, exhibits potential-dependent CO_2 reduction selectivity, which could result in temporal variation of syngas composition and limit its use in large-scale electrochemical syngas production. Herein, we demonstrate the use of Ag nanowire (NW)/porous carbon sheet composite catalysts in the generation of syngas with tunable H_2/CO ratios having a large potential window to resist power fluctuation. These Ag NW/carbon sheet composite catalysts have a potential window increased by 10 times for generating syngas with the proper H_2/CO ratio (1.7−2.15) for the Fischer−Tropsch process and an increased syngas production rate of about 19 times compared to that of a Ag foil. Additionally, we tuned the H_2/CO ratio from ∼2 to ∼10 by adjusting only the quantity of the Ag NWs under the given electrode potential. We believe that our Ag NW/carbon sheet composite provides new possibilities for designing electrode structures with a large potential window and controlled CO_2 reduction products in aqueous solutions.

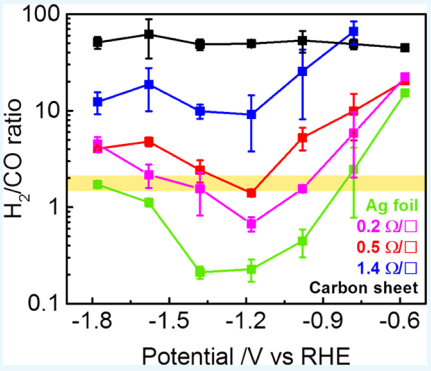

1. INTRODUCTION

Global climate change accelerated by carbon dioxide emissions has increased the demand to reduce the atmospheric CO_2 concentration by CO_2 capture, storage, and conversion.[1] Among these, CO_2 conversion technologies, such as bioconversion, electrochemical conversion, and combined reforming, have attracted much interest for converting CO_2 into value-added products.[2−4] Electrochemical CO_2 conversion can produce various fuels and carbon feedstocks, including CO, CH_4, HCOOH, and C_2H_4, at room temperature using renewable energy resources.[5,6] In particular, CO production by the electrochemical CO_2 reduction reaction (CO_2RR) is attractive because it involves only two electrons and is a main component of syngas, which is widely used to synthesize value-added hydrocarbons in various industries.[6] Syngas, a mixture of H_2 and CO, can be transformed into various hydrocarbons, such as methanol or synthetic crude oil, through the Fischer−Tropsch (F−T) process. In the F−T process, the ratio of syngas is crucial to maximize the product yield. For instance, the optimal H_2/CO ratio for syngas to generate hydrocarbons is 1.7 when using an iron-based catalyst and 2.15 when using a cobalt-based catalyst.[7,8]

Metal catalysts such as Au, Ag, and Zn can be used as electrochemical catalysts to reduce CO_2 to CO in aqueous solutions.[5,9] With these metal catalysts, syngas can be directly produced by electrochemical reduction of CO_2 to CO in aqueous solutions because electrochemical CO_2RR in an aqueous solution always accompanies the H_2 evolution reaction (HER) as a competitive reaction. However, this competitive reaction is the main reason for potential-dependent product distribution for typical CO_2RR metal catalysts. For example, in the case of Ag, the CO Faraday efficiency rapidly decreases from about 90 to <20% when the applied potential is changed from −1.02 to −0.75 V (vs reversible hydrogen electrode (RHE)), respectively, in CO_2-saturated 0.1 M $KHCO_3$.[10] This is due to the fact that the CO_2RR current density for CO generation, j_{CO}, is limited by the low solubility of CO_2 in water (34 mmol/L at 1 atm and 25 °C)[11] and the sluggish reaction kinetics, which requires a high overpotential of more than 1 V to drive a sufficiently high j_{CO}.[12] This leads to considerable generation of the HER current density, j_{H_2}, at a low overpotential. This potential-dependent H_2/CO distribution from a metal catalyst can limit the use of electrochemical CO_2RR for direct syngas production and requires additional facilities to adjust the syngas ratio. Especially in a two-electrode CO_2 electrolysis system, it is difficult to impose an exact electrode potential on a metal catalyst, and it would cause a temporal variation in the H_2/CO ratio. This becomes further aggravated if unstable electricity resources like photovoltaics and wind power are used. Therefore, to achieve cost-effective

Received: June 23, 2017
Accepted: June 30, 2017
Published: July 11, 2017

DOI: 10.1021/acsomega.7b00846
ACS Omega 2017, 2, 3441−3446

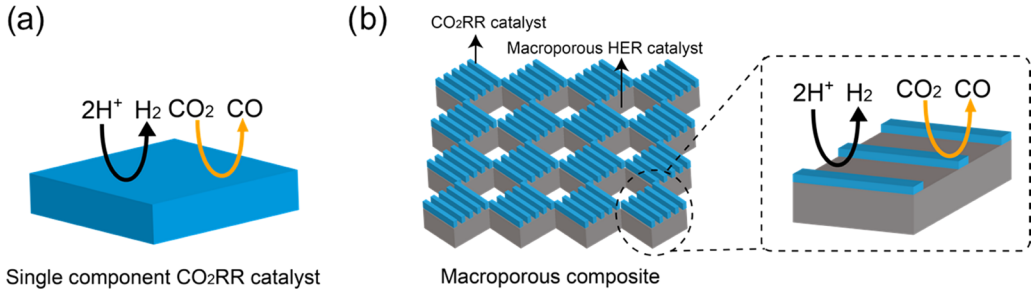

Figure 1. CO_2RR schemes from (a) single-component and (b) composite catalysts for tunable H_2/CO production during electrochemical CO_2RR electrolysis.

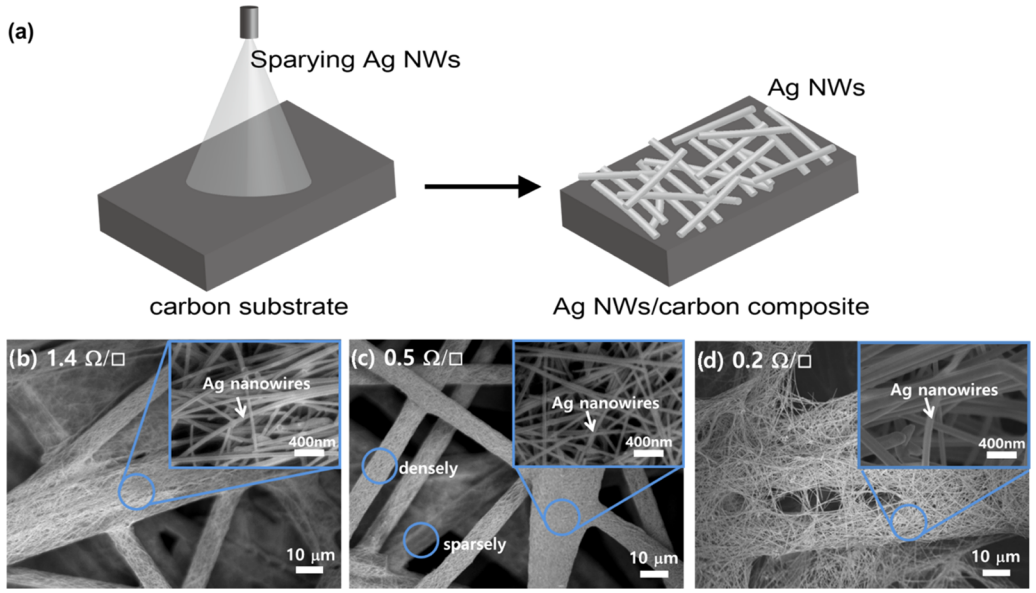

Figure 2. (a) Schematic diagram showing the fabrication of the Ag NWs/carbon sheet composite by spraying the Ag NWs; scanning electron microscope (SEM) images of the Ag NW composites with (b) 1.4 Ω/□, (c) 0.5 Ω/□, and (d) 0.2 Ω/□ of Ag NWs. The insets show enlarged images of the Ag NWs/carbon sheet composites.

and sustainable syngas production with the optimum H_2/CO ratio, it is crucial to develop a CO_2RR catalyst capable of tuning the CO_2RR and HER rates over wide ranges of operating conditions.

Thus far, the search for a single metal or bimetallic catalyst to convert CO_2 to CO has focused on achieving the maximum CO generation rate at a low overpotential by controlling nanostructures and crystal facets.[13−21] For example, nanoporous Au and Ag dramatically improve the CO_2RR activity, showing nearly 100% CO production in an aqueous solution at a low overpotential.[14,16] Also, Ag with an $In(OH)_3$ support shows a higher CO current efficiency than that of pure Ag and $In(OH)_3$.[20] In addition, Won et al. show that hexagonal Zn nanostructures with (101) crystal facets are effective in converting CO_2 to CO.[21] However, dominant CO production would require additional H_2 sources for direct syngas production. Recently, Spurgeon et al. reported on the simultaneous production of CO and H_2 with tunable H_2/CO ratios from ∼97 to 0.36 on a Cu foil by controlling the pulse times at a specific bias during pulsed-biased CO_2 electrolysis.[22] However, simultaneous H_2 and CO formation with tunable compositions relevant to syngas with a large potential window for optimum hydrocarbon production remains challenging in potentiostatic CO_2 electrolysis.

Here, we introduce porous composite materials for producing syngas with tunable H_2/CO ratios for extended ranges of electrode potentials in potentiostatic CO_2 electrolysis. Our composite material is composed of Ag nanowires (NWs) as the CO_2RR catalyst on top of a thick macroporous carbon sheet as the HER catalyst. Compared to a Ag foil, our Ag NWs/carbon sheet composites have an increased syngas production rate of about 19 times with a H_2/CO ratio of 1.7−2.15, which is optimum for the F−T process, and an increased range in the electrode potential of about 10 times during potentiostatic CO_2 electrolysis in an aqueous solution. In addition, controllability of the syngas composition from ∼0.7 to 80 was demonstrated by simply controlling the loading amount of Ag NWs.

2. RESULTS AND DISCUSSION

A schematic diagram of our composite CO_2RR catalyst for tunable H_2/CO production is shown in Figure 1. Unlike conventional single-component CO_2RR catalysts for which the competitive HER and CO_2RR occur on the same electrode surface (Figure 1a), our composite catalyst is designed to reduce CO_2 and water independently from the corresponding CO_2RR and HER catalysts following their own electrochemical characteristics. For instance, as shown in Figure 1b, CO_2 will be reduced to CO on the CO_2RR catalyst, which is on top of the macroporous HER catalyst. Then, unreacted protons will be

DOI: 10.1021/acsomega.7b00846
ACS Omega 2017, 2, 3441−3446

transported to the underlying HER catalyst for H_2 production. The macroporosity of our composite catalysts provides facile transport of protons to the HER catalyst as well as enhanced reactivity from the increased surface area. To achieve a tunable H_2/CO ratio over a wide range of electrode potentials, both the CO_2RR and HER catalysts in the composite should have similar electrochemical current density−potential (j−V) characteristics, such as the onset potentials for CO_2RR and HER, respectively. In addition, the products ratio of CO can be independently controlled by changing the loading amount of the CO_2RR catalyst. In this work, we used Ag NWs as the CO_2RR catalyst and a macroporous carbon sheet as the substrate for the Ag NWs and the HER catalyst. These Ag NWs simply enable us to tune the H_2/CO ratio by controlling the quantity of sprayed Ag NWs. Also, we chose a carbon sheet although it is known to be a poor HER catalyst because the HER onset potential of the carbon sheet is well-matched with the CO_2RR onset potential of Ag explained below.

The Ag NWs/carbon sheet composites were fabricated by spraying Ag NWs on a macroporous carbon sheet shown in Figure 2a. The synthesized Ag NWs with a 50 nm diameter and ∼30 μm length were dispersed in solution and sprayed by a sprayer previously described. After spraying, an intimate contact between each Ag NW was made by annealing at 100 °C for 60 min. The loading amount of the Ag NWs on a carbon sheet was controlled by adjusting the spraying time. To quantify the Ag NW loading amount, we measured the sheet resistance of the Ag NWs on a slide glass, which were sprayed for the same amount of time as the spraying time for the carbon sheet (see Figure S1).

Figure 2b−d shows the SEM images of the sprayed Ag NWs on the carbon sheets with different spraying times. The sheet resistances of Ag NWs on the carbon sheet are 1.4, 0.5, and 0.2 Ω/□, respectively. Hereafter, these are referred to as the 1.4 Ω/□ Ag NWs/carbon sheet composite, 0.5 Ω/□ Ag NWs/carbon sheet composite, and 0.2 Ω/□ Ag NWs/carbon sheet composite. As clearly shown in Figure 2b−d, the sprayed Ag NWs are stacked mostly at the top of the macroporous carbon sheets and form a porous structure, which creates a greater surface area for CO_2RR and could facilitate proton transfer to the bottom of the macroporous carbon sheets for HER. In addition, the Ag NWs/carbon sheet composite with a lower sheet resistance has more densely stacked Ag NWs compared to those in the Ag NW composite with a higher sheet resistance. In other words, the exposed carbon sheet surface area of the topmost region toward electrolyte would be decreased as lowering the Ag NWs/carbon sheet composite sheet resistance. This means that the reaction areas for HER and CO_2RR are controlled by the quantity of Ag NWs, spontaneously. Therefore, the evolution ratio of H_2 and CO through the Ag NWs/carbon sheet composites is adjustable by controlling the amount of Ag NWs. The X-ray photoelectron spectroscopy (XPS) spectrum of the Ag NWs/carbon sheet composites shows peaks at 368.2 and 374.2 eV, indicating no significant surface chemical state changes during the spraying or annealing process (Figure S2). To figure out the CO_2RR property of Ag NWs themselves, we sprayed different amounts of Ag NWs on Ag foils by adjusting the spraying time. If the activity of Ag NWs for CO_2RR is different from that of a Ag foil, CO selectivity and electrochemical properties, such as Tafel slope, partial current density (j_{CO}), and total current density (j_{total}), of Ag NWs sprayed on Ag foil electrodes would be changed with increasing the quantity of sprayed Ag NWs. However, all of the "Ag NWs on the Ag foil" electrodes and the bare Ag foil had a similar CO selectivity and Tafel slope (∼180 mV/decade) as a function of the applied potential (Figures S3−S5) despite different Ag NWs quantities. The similar CO_2RR characteristics of Ag NWs and Ag foils are believed, mainly, due to the exposed crystal facets of Ag NWs. According to our previous work, our sprayed Ag NWs are single crystalline with the growth direction of {110}: the (100) and (111) facets are mostly exposed in our sprayed Ag NWs.[23,26] Polycrystalline Ag also mainly expose the (100) and (111) facets rather than (110) because of its low surface energy.[27−29] Because the Ag(100) and Ag(111) facets are known to have similar CO_2RR properties,[30] no significant CO_2RR property difference between our Ag NWs and an Ag foil was observed from the CO_2RR performance of the Ag NWs sprayed onto the Ag foil.

To briefly look into the electrode characteristics, linear sweep voltammetry (LSV) was conducted in a CO_2-saturated 0.2 M $KHCO_3$ aqueous solution (Figure 3). As clearly shown in Figure 3, bare Ag foil and bare carbon sheet show a similar voltage onset of about −0.79 V, although the bare carbon sheet has a higher current density than that of the bare Ag. Interestingly, Ag NWs/carbon sheet composites also have a similar voltage onset of about −0.79 V but exhibit different current densities depending on the Ag NW loadings. Because of the higher exposed surface area of the carbon sheet, for example, the 1.4 Ω/□ Ag NWs/carbon sheet composite has a more carbon sheet like j−V behavior than that of the 0.5 or 0.2 Ω/□ Ag NWs/carbon sheet composite shown in Figure 3. Note that the LSV curve of the Ag foil shows a similar behavior as that in previously reported results.[10]

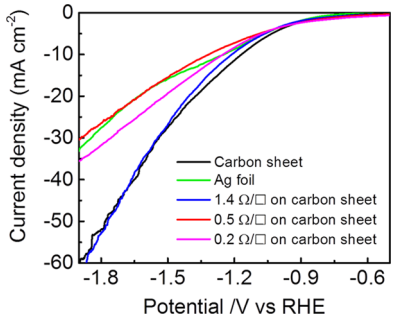

Figure 3. LSV of the carbon sheet, Ag foil, and Ag NWs/carbon sheet composites with 1.4, 0.5, and, 0.2 Ω/□ of Ag NWs in CO_2-saturated 0.2 M $KHCO_3$.

Gas chromatography (GC) showed a dramatic difference in the j_{H_2} and j_{CO} compositions depending on the applied potentials. Figure 4a−e shows the partial current densities for HER and CO_2RR of the five electrodes extracted from the chronoamperometry. All data points were converted from the current density−time curves in Figure S6, and 0.1−0.5 C charge was passed through the electrode surfaces. The total Faraday efficiencies of all electrodes are shown in Figure S7. As seen in Figure 4a, the Ag foil has a typical potential-dependent CO_2RR activity, as reported elsewhere. For instance, the j_{CO} of the Ag foil starts to increase at about −0.79 V and becomes saturated at ∼10 mA/cm^2 when the applied potential is more negative than −1.39 V. The j_{H_2} of the Ag foil is suppressed up to −1.39 V and then rapidly increases. Therefore, the H_2/CO production ratio is highly dependent on the applied potentials. In contrast, a carbon sheet produces mostly j_{H_2} with a potential

DOI: 10.1021/acsomega.7b00846
ACS Omega 2017, 2, 3441−3446

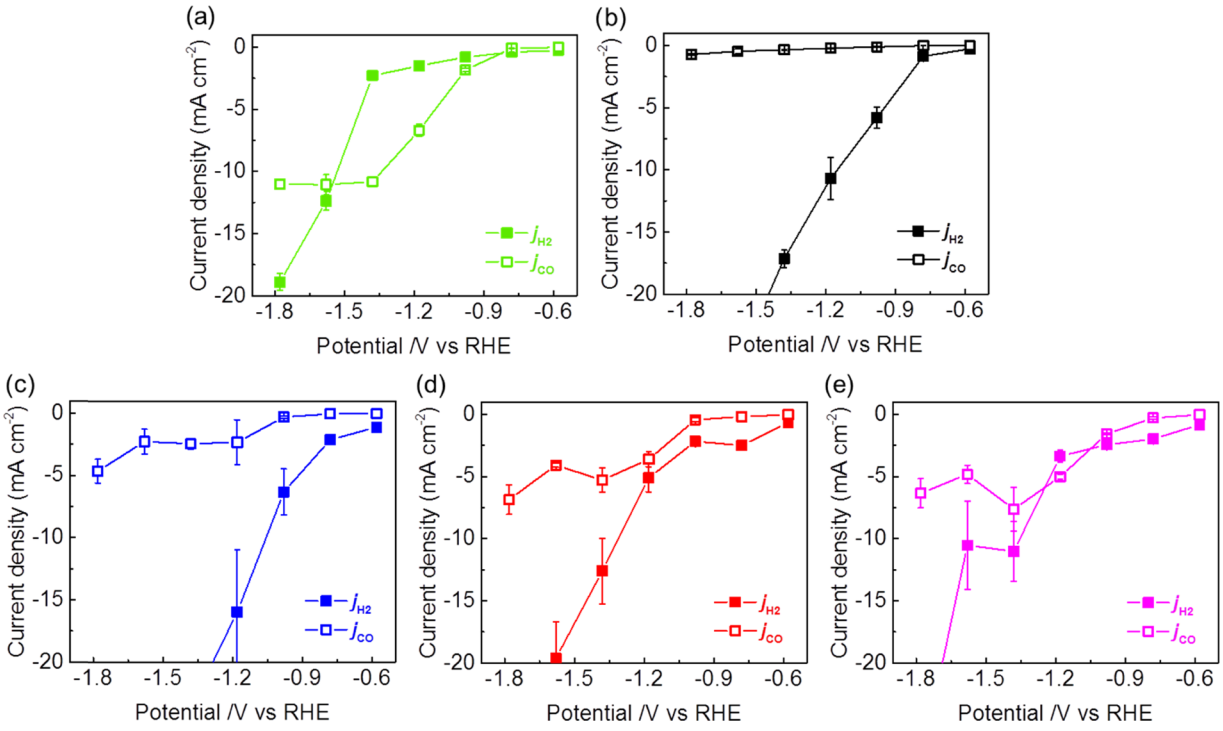

Figure 4. Partial current densities j_{H_2} and j_{CO} of (a) Ag foil, (b) carbon sheet, (c) 1.4 Ω/□ Ag NWs/carbon sheet composite, (d) 0.5 Ω/□ Ag NWs/carbon sheet composite, and (e) 0.2 Ω/□ Ag NWs/carbon sheet composite.

onset of about −0.79 V. Note that the bare Ag foil and carbon sheet show a similar onset potential of about −0.79 V for CO_2RR and HER, respectively. When the Ag NWs are deposited onto a carbon sheet, the j_{CO} starts to increase, which is affected by the loading amount of Ag NWs. For instance, the j_{CO} of the Ag NWs/carbon sheet composites at −1.79 V increases to ∼6 from ∼2 mA/cm^2 with increasing Ag NW loading, as shown in Figure 4c−e. Note that the j_{H_2} of the Ag NWs/carbon sheet composites originates mostly from the carbon sheets underneath the sprayed Ag NWs when the applied potential is more positive than −1.39 V. Therefore, j_{H_2} of the Ag NWs/carbon sheet composites decreases with increasing amount of sprayed Ag NWs as the exposed carbon sheet surfaces, that is, the sites for HER, are blocked by the sprayed Ag NWs. Hence, in contrast to that of the Ag foil, the partial current density difference between j_{CO} and j_{H_2} of the Ag NWs/carbon sheet composites is dramatically decreased with the 0.2 Ω/□ Ag NWs around −1.2 V. Moreover, the partial current density difference can be adjusted in accordance with the amount of Ag NWs: the 1.4 Ω/□ Ag NWs/carbon sheet composite has small changes in the partial current density gap compared to those in the 0.2 Ω/□ Ag NWs/carbon sheet composite (Figure 4c,e). This leads to a tunable H_2/CO ratio as a function of the Ag NW loading for a large range of applied potentials.

Figure 5 shows the electrochemically generated H_2/CO syngas ratios of the Ag NWs/carbon sheet composites with various applied potentials. The yellow box indicates the optimum syngas ratio (1.7−2.15) for transforming syngas to hydrocarbons by the F−T process. As clearly seen in Figure 5, the H_2/CO ratio is controlled by the amount of Ag NW loading for all potentials: at −1.2 V, the H_2/CO ratio is tuned depending on the quantity of loaded Ag NWs. More

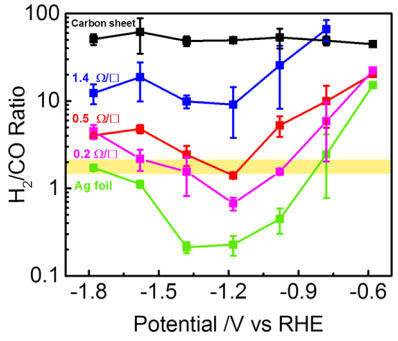

Figure 5. H_2/CO ratio from the carbon sheet, Ag foil, and Ag NWs/carbon sheet composites with different Ag NW loadings as a function of the applied potential in a CO_2-saturated 0.2 M $KHCO_3$ solution.

importantly, the Ag NWs/carbon sheet composite can generate syngas at the optimum H_2/CO ratio for the F−T process with a higher current density and under larger potential ranges than those of the Ag foil. For instance, the 0.5 Ω/□ Ag NWs/carbon sheet composite has around a 300 mV potential window for the optimal syngas ratio range, whereas the Ag foil has only around a 30 mV potential window. Moreover, the 0.5 Ω/□ Ag NWs/carbon sheet composite generates syngas at a ratio of 2.15 with a higher production rate of about 19 times compared to that of the Ag foil: the total current densities to produce H_2/CO at a ratio of 2.15 from the 0.5 Ω/□ Ag NWs/carbon sheet composite and the Ag foil are ∼8.72 and ∼0.45 mA/cm^2, respectively. In Table S1, we summarize the electrocatalytic syngas production performances of Ag-based composite materials reported in the literature. As clearly seen in Table S1, our Ag NWs/carbon sheet composite is one of the best syngas-producing composite catalysts with the highest syngas-producing current density with wide potential ranges.

DOI: 10.1021/acsomega.7b00846
ACS Omega 2017, 2, 3441−3446

Our study shows a new composite catalyst structure for generating syngas with tunable H_2/CO ratios for a wide range of electrode potentials in an aqueous electrolyte. However, our Ag NWs/carbon sheet composite still suffers from high overpotentials and a small j_{total} for large-scale application. To lower the overpotentials in our composite catalyst, the Ag NWs need to be replaced with other catalyst materials with low CO_2RR overpotentials, such as oxide-derived Au or Au nanoneedles.[16,31] In this case, of course, substrates with a smaller HER onset potential, such as C_3N_4@N-graphene or PCN@N-graphene, are needed for tunable H_2/CO production.[32,33] In addition, the j_{total} can be enhanced by lowering the electrolyte temperatures or increasing the reactor pressure to increase the CO_2 solubility in an aqueous solution, which is the main reason for the low CO_2RR current density. Alternatively, the CO_2 solubility can be enhanced by adding additives, such as ionic liquids, in an aqueous solution or using a nonaqueous electrolyte.[34]

3. CONCLUSIONS

We present a strategy to develop an electrocatalyst to produce syngas with controllable H_2/CO ratios by independently providing reaction sites for HER and CO_2RR during electrochemical CO_2RR in an aqueous solution. Ag NWs/macroporous carbon composites were selected by considering each electrochemical performance of the carbon and Ag for HER and CO_2RR and prepared by spraying the Ag NWs onto a carbon sheet. In our composite, the H_2/CO ratio is controlled simply by changing the Ag NW loading on the carbon sheet. Our Ag NWs/carbon sheet composite has potential ranges that are 10 times larger for the generation of syngas with the optimum ratio for the F−T process (from 1.7 to 2.15) and a syngas production rate that is about 19 times higher than that of Ag foil. Finally, we believe that, by identifying composite materials with low overpotentials for HER and CO_2RR as well as further engineering of electrolytes for enhanced CO_2 solubility, our composite electrocatalyst design could be used to produce syngas with a tunable H_2/CO ratio by electrochemical CO_2RR using renewable energy resources in large-scale applications.

4. EXPERIMENTAL SECTION

4.1. Electrode Preparation. Ag NWs were synthesized by the modified polyol process described previously.[23] The solution of synthesized Ag NWs was sprayed onto the carbon sheet (TGP-H; Toray Industries, Inc.) with a spray system to fabricate a Ag NW network structure. The amount of Ag NWs on the carbon sheet was monitored by measuring the sheet resistance of the Ag NWs on a glass substrate, which was prepared at the same time. The relationship between the sheet resistance and the quantity of Ag NWs (mg/cm^2) is shown in Figure S1. After the spraying, the carbon sheet was placed on a 100 °C hot plate to evaporate the solvent.[24] The Ag NWs/carbon sheet composites with different sheet resistances were fabricated by varying the spraying time of the Ag NW solution. The Ag foil (99.998%; Alfa Aesar) was mechanically polished with sandpaper (CC-400Cw; Daesung) and dipped into a 0.1 M H_2SO_4 aqueous solution overnight to remove any organic impurities on the metal surface before the CO_2RR.[25] All prepared electrodes with an attached copper wire on the back side were sealed by industrial epoxy (Loctite 9460) to confine the reactive area. The geometric surface area of the exposed electrode was then determined by an image processing program (ImageJ) with scanned images (300 dpi resolution).

4.2. Electrochemical Experiments and Product Analysis. All electrochemical experiments were performed with a gas-tight single-compartment electrolysis cell. The total volume of the single-compartment cell was 60 mL with 20 mL of 0.2 M $KHCO_3$ (99.95%; Sigma-Aldrich) and a 40 mL head space. A Ag/AgCl (3 M NaCl) electrode and a graphite rod were used as a reference electrode and a counter electrode, respectively. The reference electrode potentials were converted to RHE with equation E as follows: (RHE) = E (Ag/AgCl) + 0.209 V + 0.0591 V × pH. Prior to the CO_2RR electrochemical experiment, a 100 mL/min stream of CO_2 gas (99.999%) was purged for at least 30 min to saturate the electrolyte with CO_2 and the pH of the solution was 6.8. The electrolyte solution was stirred by a magnetic bar during the experiments. The electrochemical properties of the electrodes were measured with a potentiostat (SP-150; Bio-Logic Science Instruments). LSV curves for each electrode were scanned from −0.3 to −1.8 V with a scan rate of 50 mV/s. The quantification of the gas product was analyzed by GC (micro GC 3000; INFICON) equipped with a thermal conductor detector. Argon (99.9999%) and helium (99.9999%) were used as carrier gases for a PLOT Q and molecular sieve column, respectively. All gas products were generated by constant potential electrolysis at seven different potentials. The gas-phase products were directly injected from the single-compartment cell into the GC column to minimize the contamination of the collected gas product.

4.3. Microscopy Measurement. The surface morphologies of the Ag NWs/carbon sheet composite and carbon sheet were observed by a SEM (JEOL-7600F) operated at 5 kV. The surface state of the five different electrodes was observed by XPS (Thermo Scientific K-alpha).

■ ASSOCIATED CONTENT

Supporting Information

The Supporting Information is available free of charge on the ACS Publications website at DOI: 10.1021/acsomega.7b00846.

XPS; gas product analysis results; partial current density; chronoamperometry data information (PDF)

■ AUTHOR INFORMATION

Corresponding Authors

*E-mail: jungyong.lee@kaist.ac.kr (J.-Y.L.).
*E-mail: jihun.oh@kaist.ac.kr (J.O.).

ORCID

Jihun Oh: 0000-0001-6465-6736

Author Contributions

The manuscript was written through contributions of all authors. All authors have given approval to the final version of the manuscript.

Notes

The authors declare no competing financial interest.

■ ACKNOWLEDGMENTS

This work was supported by a grant from the Korea CCS R&D Center (KCRC) funded by the Korean government (Ministry of Science, ICT and Future Planning) (NRF-2014M1A8A1049303).

DOI: 10.1021/acsomega.7b00846
ACS Omega 2017, 2, 3441−3446

REFERENCES

(1) Cox, P. M.; Betts, R. A.; Jones, C. D.; Spall, S. A.; Totterdell, I. J. Acceleration of global warming due to carbon-cycle feedbacks in a coupled climate model. *Nature* **2000**, *408*, 184−187.

(2) Budiman, A. W.; Song, S.-H.; Chang, T.-S.; Shin, C.-H.; Choi, M.-J. Dry Reforming of Methane Over Cobalt Catalysts: A Literature Review of Catalyst Development. *Catal. Surv. Asia* **2012**, *16*, 183−197.

(3) Brennan, L.; Owende, P. Biofuels from microalgae—A review of technologies for production, processing, and extractions of biofuels and co-products. *Renewable Sustainable Energy Rev.* **2010**, *14*, 557−577.

(4) White, J. L.; Baruch, M. F.; Pander, J. E., III; Hu, Y.; Fortmeyer, I. C.; Park, J. E.; Zhang, T.; Liao, K.; Gu, J.; Yan, Y.; et al. Light-Driven Heterogeneous Reduction of Carbon Dioxide: Photocatalysts and Photoelectrodes. *Chem. Rev.* **2015**, *115*, 12888−12935.

(5) Hori, Y. *Electrochemical CO_2 Reduction on Metal Electrodes*; Springer, 2008; Vol. *42*.

(6) Durst, J.; Rudnev, A.; Dutta, A.; Fu, Y.; Herranz, J.; Kaliginedi, V.; Kuzume, A.; Permyakova, A. A.; Paratcha, Y.; Broekmann, P.; Schmidt, T. J. Electrochemical CO_2 Reduction−A Critical View on Fundamentals, Materials and Applications. *CHIMIA Int. J. Chem.* **2015**, *69*, 769−776.

(7) Dry, M. E. High quality diesel via the Fischer−Tropsch process − a review. *J. Chem. Technol. Biotechnol.* **2002**, *77*, 43−50.

(8) Gutierrez, R. R.; Haussener, S. Modeling of Concurrent CO_2 and Water Splitting by Practical Photoelectrochemical Devices. *J. Electrochem. Soc.* **2016**, *163*, H1008−H1018.

(9) Kuhl, K. P.; Hatsukade, T.; Cave, E. R.; Abram, D. N.; Kibsgaard, J.; Jaramillo, T. F. Electrocatalytic Conversion of Carbon Dioxide to Methane and Methanol on Transition Metal Surfaces. *J. Am. Chem. Soc.* **2014**, *136*, 14107−14113.

(10) Hatsukade, T.; Kuhl, K. P.; Cave, E. R.; Abram, D. N.; Jaramillo, T. F. Insights into the electrocatalytic reduction of CO_2 on metallic silver surfaces. *Phys. Chem. Chem. Phys.* **2014**, *16*, 13814−13819.

(11) Dodds, W.; Stutzman, L.; Sollami, B. Carbon Dioxide Solubility in Water. *Ind. Eng. Chem. Chem. Eng. Data Ser.* **1956**, *1*, 92−95.

(12) Whipple, D. T.; Kenis, P. J. Prospects of CO_2 Utilization via Direct Heterogeneous Electrochemical Reduction. *J. Phys. Chem. Lett.* **2010**, *1*, 3451−3458.

(13) Kim, C.; Jeon, H. S.; Eom, T.; Jee, M. S.; Kim, H.; Friend, C. M.; Min, B. K.; Hwang, Y. J. Achieving Selective and Efficient Electrocatalytic Activity for CO2 Reduction Using Immobilized Silver Nanoparticles. *J. Am. Chem. Soc.* **2015**, *137*, 13844−13850.

(14) Lu, Q.; Rosen, J.; Zhou, Y.; Hutchings, G. S.; Kimmel, Y. C.; Chen, J. G.; Jiao, F. A selective and efficient electrocatalyst for carbon dioxide reduction. *Nat. Commun.* **2014**, *5*, No. 3242.

(15) Back, S.; Yeom, M. S.; Jung, Y. Active Sites of Au and Ag Nanoparticle Catalysts for CO_2 Electroreduction to CO. *ACS Catal.* **2015**, *5*, 5089−5096.

(16) Chen, Y.; Li, C. W.; Kanan, M. W. Aqueous CO_2 Reduction at Very Low Overpotential on Oxide-Derived Au Nanoparticles. *J. Am. Chem. Soc.* **2012**, *134*, 19969−19972.

(17) Lee, C. H.; Kanan, M. W. Controlling H^+ vs CO_2 Reduction Selectivity on Pb Electrodes. *ACS Catal.* **2015**, *5*, 465−469.

(18) Li, C. W.; Kanan, M. W. CO_2 Reduction at Low Overpotential on Cu Electrodes Resulting from the Reduction of Thick Cu_2O Films. *J. Am. Chem. Soc.* **2012**, *134*, 7231−7234.

(19) Lates, V.; Falch, A.; Jordaan, A.; Peach, R.; Kriek, R. J. An electrochemical study of carbon dioxide electroreduction on gold-based nanoparticle catalysts. *Electrochim. Acta* **2014**, *128*, 75−84.

(20) Larrazábal, G. O.; Martín, A. J.; Mitchell, S.; Hauert, R.; Pérez-Ramírez, J. Synergistic effects in silver−indium electrocatalysts for carbon dioxide reduction. *J. Catal.* **2016**, *343*, 266−277.

(21) Won, D. H.; Shin, H.; Koh, J.; Chung, J.; Lee, H. S.; Kim, H.; Woo, S. I. Highly Efficient, Selective, and Stable CO_2 Electroreduction on a Hexagonal Zn Catalyst. *Angew. Chem., Int. Ed.* **2016**, *55*, 9297−9300.

(22) Kumar, B.; Brian, J. P.; Atla, V.; Kumari, S.; Bertram, K. A.; White, R. T.; Spurgeon, J. M. Controlling the Product Syngas H_2: CO Ratio through Pulsed-bias Electrochemical Reduction of CO_2 on Copper. *ACS Catal.* **2016**, *6*, 4739−4745.

(23) Yang, C.; Gu, H.; Lin, W.; Yuen, M. M.; Wong, C. P.; Xiong, M.; Gao, B. Silver Nanowires: from Scalable Synthesis to Recyclable Foldable Electronics. *Adv. Mater.* **2011**, *23*, 3052−3056.

(24) Lee, J.; Lee, I.; Kim, T. S.; Lee, J. Y. Efficient Welding of Silver Nanowire Networks without Post-Processing. *Small* **2013**, *9*, 2887−2894.

(25) Salehi-Khojin, A.; Jhong, H.-R. M.; Rosen, B. A.; Zhu, W.; Ma, S.; Kenis, P. J.; Masel, R. I. Nanoparticle Silver Catalysts That Show Enhanced Activity for Carbon Dioxide Electrolysis. *J. Phys. Chem. C* **2013**, *117*, 1627−1632.

(26) Liu, X.; Luo, J.; Zhu, J. Size Effect on the Crystal Structure of Silver Nanowires. *Nano Lett.* **2006**, *6*, 408−412.

(27) Wang, S. G.; Tian, E. K.; Lung, C. W. Surface energy of arbitrary crystal plane of bcc and fcc metals. *J. Phys. Chem. Solids* **2000**, *61*, 1295−1300.

(28) Uda, M.; Nakamura, A.; Yamamoto, T.; Fujimoto, Y. Work function of polycrystalline Ag, Au and Al. *J. Electron Spectrosc. Relat. Phenom.* **1998**, *88*−*91*, 643−648.

(29) Zoo, Y.; Alford, T. Comparison of preferred orientation and stress in silver thin films on different substrates using x-ray diffraction. *J. Appl. Phys.* **2007**, *101*, No. 033505.

(30) Hoshi, N.; Kato, M.; Hori, Y. Electrochemical reduction of CO_2 on single crystal electrodes of silver Ag (111), Ag (100) and Ag (110). *J. Electroanal. Chem.* **1997**, *440*, 283−286.

(31) Liu, M.; Pang, Y.; Zhang, B.; De Luna, P.; Voznyy, O.; Xu, J.; Zheng, X.; Dinh, C. T.; Fan, F.; Cao, C.; et al. Enhanced electrocatalytic CO_2 reduction via field-induced reagent concentration. *Nature* **2016**, *537*, 382−386.

(32) Zheng, Y.; Jiao, Y.; Zhu, Y.; Li, L. H.; Han, Y.; Chen, Y.; Du, A.; Jaroniec, M.; Qiao, S. Z. Hydrogen evolution by a metal-free electrocatalyst. *Nat. Commun.* **2014**, *5*, No. 3783.

(33) Duan, J.; Chen, S.; Jaroniec, M.; Qiao, S. Z. Porous C_3N_4 nanolayers@ N-graphene Films as Catalyst Electrodes for Highly Efficient Hydrogen Evolution. *ACS Nano* **2015**, *9*, 931−940.

(34) Koh, J. H.; Jeon, H. S.; Jee, M. S.; Nursanto, E. B.; Lee, H.; Hwang, Y. J.; Min, B. K. Oxygen Plasma Induced Hierarchically Structured Gold Electrocatalyst for Selective Reduction of Carbon Dioxide to Carbon Monoxide. *J. Phys. Chem. C* **2015**, *119*, 883−889.

DOI: 10.1021/acsomega.7b00846
ACS Omega 2017, 2, 3441−3446